Volume Averaging Technique for Deep-Mixed Columns under Embankments: Verification and Validation

Volume Averaging Technique for Deep-Mixed Columns under Embankments: Verification and Validation

Ayman Abed[1]; Urs Vogler[2]; and Minna Karstunen[3]

Abstract: Modeling the three-dimensional (3D) soil–structure interaction of geostructures on periodic ground improvement, in order to optimize the design, is a computationally demanding task. Thus, this paper exploits the so-called volume averaging technique (VAT), an attractive numerical tool to represent the composite material behavior by homogenizing the problem yet having two independent constitutive models for the constituents involved. The derived formulation for the averaged material behavior of the column improved ground enables to map this fully 3D problem into an equivalent two-dimensional (2D) plane-strain counterpart. After discussing the theoretical framework and the underlying assumptions, the numerical implementation of the technique is explained in detail. The trial embankments in Paimio, Finland, were modeled as full 3D problems as well as using the volume averaging technique in 2D plane-strain conditions. The excellent match between the 3D simulation results and that by the VAT verified the framework and the implementation. Furthermore, the technique was validated by being able to replicate the measured data with very good accuracy. **DOI: 10.1061/IJGNAI.GMENG-11450**.

Author keywords: Homogenization; Constitutive modeling; Finite-element method; Deep mixing; Soft clay; Paimio trial embankments.

Introduction

Due to increasing urbanization, the possibilities to construct on the ground with appropriate engineering properties are becoming limited. Furthermore, the designer is forced to deal with the challenges associated with difficult soils, such as soft clay, in terms of low shear strength and excessive deformations. Among the design alternatives, stabilizing the soil (i.e., increasing its stiffness and strength) by the deep mixing technique with a suitable binder (e.g., cement and/or lime) (Broms and Boman 1979) is gaining popularity for its economic feasibility and environmental friendliness by saving a significant amount of the used binder and consequently reducing CO_2 emission, in comparison to other improvement alternatives. Roads and railroad embankments represent typical applications for deep mixing. However, the designer, who is seeking the diameter, the spacing, and the arrangement of the columns that satisfy both serviceability (SLS) and ultimate limit state (ULS) requirements, will be facing a complex, fully three-dimensional (3D) problem. Existing design methods rely on simplified assumptions, such as elasticity, to estimate settlements under working loads and rigid-perfectly plastic solutions for ultimate load at failure (EuroSoilStab 2002), leading to overconservative solutions in most cases. For instance, in a recent study, Savila et al. (2025) examined recovered field samples from multiple column stabilization sites. The findings revealed that the shear strength of the recovered stabilized samples was 7–20 times greater than the target strength (100–140 kPa) set in the design. Consequently, the guideline values for strength and stiffness ratios (natural soil versus stabilized soil) are routinely exceeded. Alternatively, one can use the FEM as a more advanced design tool that offers the possibility not only to capture accurately the main features of natural clay behavior, including anisotropy, bonding, and creep (Sivasithamparam et al. 2015; Gras et al. 2018), but also the behavior of improved columns in terms of stiffness nonlinearity and plasticity. However, the three-dimensional nature of the problem makes the 3D analysis very expensive computationally. For instance, it requires the modeling of each individual column as a volume element, leading to a very high number of degrees of freedom to be solved (Abed et al. 2021). To cope with this problem, benefiting from the periodic nature of deep mixing, this paper discusses the so-called volume averaging technique (VAT) to substitute the composite mixed column-ground material by an equivalent homogenized material, enabling the transformation of the actual 3D problem into an equivalent two-dimensional (2D) plane-strain counterpart. The method preserves all the advantages of the 3D calculations related to the advanced constitutive modeling of the soil and the columns and the flexibility in treating arbitrary loadings and boundary conditions while reducing the computational effort tremendously.

In fact, the idea of homogenization is not new because it was proposed by several authors with different approaches. For instance, Canetta and Nova (1989) proposed macroscopic yield conditions to capture the strength of the improved material using averaged strength parameters. Schweiger (1989) and Schweiger and Pande (1986, 1989) proposed a more elegant method by averaging the elastic properties according to the volume fractions and assigning different yield criteria for each constituent during plasticity. Later, Lee (1993) and Lee and Pande (1998) formulated an equivalent elastic material stiffness matrix based on the individual stiffness matrices of the constituents and their volume fractions. Like Schweiger and Pande (1986, 1989), they used different yield functions during plasticity. The formulation ensured local equilibrium between the columns and the surrounding soil at

[1]Senior Lecturer, Dept. of Architecture and Civil Engineering, Chalmers Univ. of Technology, Gothenburg SE-412 96, Sweden (corresponding author). ORCID: https://orcid.org/0000-0002-5336-3046. Email: ayman.abed@chalmers.se

[2]Team Leader Safety, DNV SE, Maritime, Hamburg 20457, Germany. Email: urs_vogler@gmx.de

[3]Professor, Dept. of Architecture and Civil Engineering, Chalmers Univ. of Technology, Gothenburg SE-412 96, Sweden. ORCID: https://orcid.org/0000-0002-5401-5721. Email: minna.karstunen@chalmers.se

Note. This manuscript was submitted on October 17, 2024; approved on July 2, 2025; published online on November 12, 2025. Discussion period open until April 12, 2026; separate discussions must be submitted for individual papers. This paper is part of the ***International Journal of Geomechanics***, © ASCE, ISSN 1532-3641.

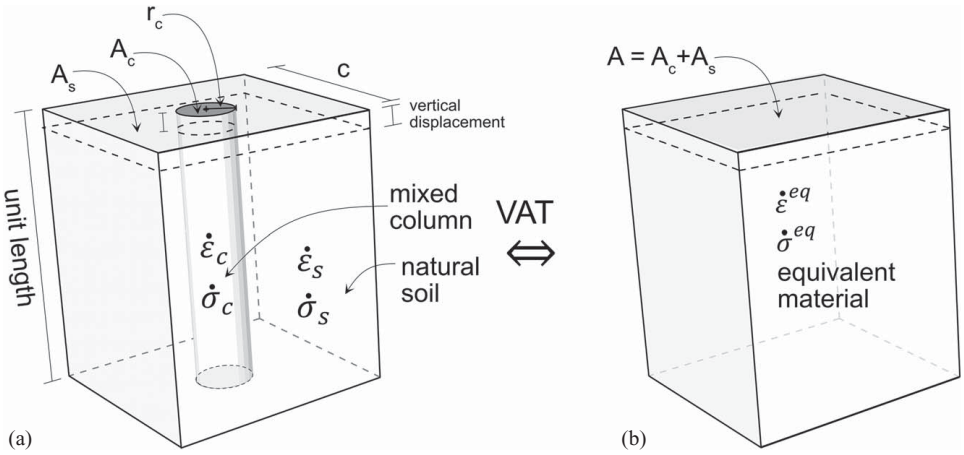

Fig. 1. Unit cell of deep-mixed soil: (a) individual components; and (b) equivalent homogenization material.

least during elasticity but offered no check on that in case of plasticity. Following the same line of research, Vogler and Karstunen (2007, 2008) and Vogler (2008) developed the technique so that local equilibrium is satisfied even during plasticity. Their formulation also considered pore-water pressure and the consolidation process. Becker and Karstunen (2013, 2014) highlighted the accuracy and the limitations of the method in terms of the number of columns and the stiffness ratio between columns and soft soil.

This paper revisits the volume averaging technique by discussing the theoretical background and the underlying assumptions. Then, the steps of numerical implementation into a finite-element code are explained in detail. Finally, the trial embankments on deep-mixed columns in Paimio, Finland (Vepsäläinen and Arkima 1992) are modeled one time as a full 3D problem and another time as a 2D plane-strain problem using the VAT. The excellent match between the 3D and 2D results verified the theoretical assumptions and the numerical implementation of the method, while the very good replication of the measured data validated this attractive technique.

Novelty and Limitations

The novelty of this work lies in its innovative application and validation of the VAT for modeling complex 3D soil–structure interactions in the case of periodic deep-mixed columns under embankments. While the efficient 3D to 2D mapping and advanced homogenization of material behavior are revised in more detail within the paper, this study makes significant contributions in the following key areas:

1. It establishes a comprehensive theoretical framework by providing a detailed and thorough theoretical framework for VAT application in geotechnical contexts, including a critical analysis of the underlying assumptions. By laying a solid foundation, it significantly enhances the understanding and broadens the potential applications of the VAT in geomechanics.
2. It enables verification and validation by presenting a detailed verification process, comparing full 3D simulations with VAT-based 2D plane-strain models, effectively demonstrating the accuracy of the technique. Importantly, the study goes a step further by validating the approach with real-world data from the Paimio trial embankments in Finland, showcasing its practical applicability in real geotechnical projects.
3. It highlights the potential for optimization in the design and modeling of complex geostructures. By enabling efficient and accurate simulations, the research opens new possibilities for cost-effective and sustainable solutions in ground improvement projects, making it a valuable tool for future geotechnical engineering advancements.

At the same time, the method has the following limitations:

1. The current version of the method is limited to deep-mixed columns with periodic distributions. In cases of irregular column arrangements, a full 3D analysis is recommended.
2. The proposed framework may not apply if the stiffness differences between the columns and the soft soil become excessive, e.g., one cannot use volume averaging for modeling embankment piles.
3. The method should only be applied for the serviceability limit state because the assumed equilibrium and kinematic conditions are no longer valid when approaching failure. Near failure, soil arching can lead to the formation of shear bands, strain localization patterns, and bending failure mechanisms that are not accounted for by the underlying assumptions of the method.
4. Since the method is intended for practical application, it incorporates the fundamental assumption of equal vertical displacement for the soil and the mixed columns under the embankment, aligning with the assumptions used in existing design approaches (EuroSoilStab 2002). It is important to note, however, that this paper aims to introduce a methodology that can serve as a foundation for homogenizing various types of interactions by incorporating appropriate mechanical balance and kinematic constraints.

The following section elaborates on the theoretical basis of the method.

Volume Averaging Technique

The VAT is a numerical homogenization technique that can be employed to represent the behavior of a composite material by an equivalent uniform material. Vogler (2008), being inspired by the early work of Schweiger and Pande (1986), Lee (1993), and Lee and Pande (1998), adopted the VAT to model the behavior of deep-mixed columns and the surrounding untreated natural soil assuming an equivalent homogenized material (Fig. 1). For the sake of simplicity, in what follows, the word column implicitly refers to the binder-mixed soil column, while soil refers to the natural untreated soil.

The VAT is based on the following fundamental averaging equation (Lee 1993; Lee and Pande 1998):

$$\dot{\boldsymbol{\sigma}}^{\mathrm{eq}} = \Omega_c \dot{\boldsymbol{\sigma}}^{c} + \Omega_s \dot{\boldsymbol{\sigma}}^{s} \tag{1}$$

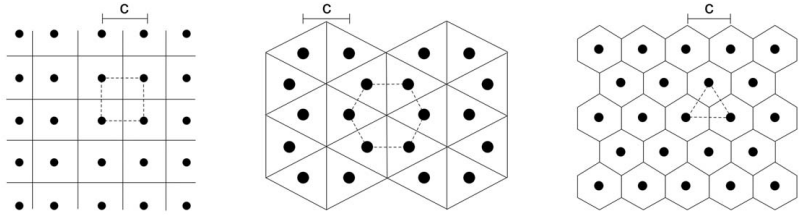

rectangular pattern | hexagonal pattern | triangular pattern

$$\Omega_c = \pi \frac{r_c^2}{c^2} \qquad \Omega_c = \sqrt{\frac{16}{27}} \pi \frac{r_c^2}{c^2} \qquad \Omega_c = \sqrt{\frac{4}{3}} \pi \frac{r_c^2}{c^2}$$

Fig. 2. Volume fraction of the column for different patterns derived based on Balaam and Booker (1981).

where $\dot{\boldsymbol{\sigma}}^{\text{eq}}$ = averaged total stress rate in the equivalent homogenization material; $\dot{\boldsymbol{\sigma}}^{c}$ and $\dot{\boldsymbol{\sigma}}^{s}$ = total stress rates in the column and the soil, respectively; and symbols Ω_c and Ω_s = so-called volume fractions of the column and the soil, respectively. They represent the relative contribution of each component in resisting the applied forces. For a vertical unit cell (Fig. 1), these fractions can be simply written as

$$\Omega_c = \frac{V_c}{V} = \frac{1 \times A_c}{1 \times A} = \frac{A_c}{A}; \quad \Omega_s = \frac{A_s}{A} \quad \text{with } \Omega_c + \Omega_s = 1 \tag{2}$$

where V and V_c = total volume of the unit cell and the volume occupied by the column, respectively; and A, A_c, and A_s = cross-sectional areas of the unit cell, the column, and the soil, respectively.

In fact, the geometric arrangement of the columns affects the value of the volume fraction. For instance, Fig. 2 presents the formulae to estimate the volume fraction for the most common arrangement patterns based on Balaam and Booker (1981). The column volume fraction Ω_c is estimated in terms of c, the center-to-center distance between columns, and the column radius r_c. Once Ω_c is estimated, the soil volume fraction Ω_s can be directly estimated from Eq. (2), where $\Omega_s = 1 - \Omega_c$.

Similar to Eq. (1), the equivalent strain rate $\dot{\boldsymbol{\varepsilon}}^{\text{eq}}$ reads

$$\dot{\boldsymbol{\varepsilon}}^{\text{eq}} = \Omega_c \dot{\boldsymbol{\varepsilon}}^{c} + \Omega_s \dot{\boldsymbol{\varepsilon}}^{s} \tag{3}$$

where $\dot{\boldsymbol{\varepsilon}}^{c}$ and $\dot{\boldsymbol{\varepsilon}}^{s}$ = strain rates in the column and the soil, respectively. Consequently, Eq. (1) can be developed further by introducing a suitable constitutive stress–strain relationship of the form $\dot{\boldsymbol{\sigma}} = \mathbf{D}\dot{\boldsymbol{\varepsilon}}$, yielding

$$\mathbf{D}^{\text{eq}} \dot{\boldsymbol{\varepsilon}}^{\text{eq}} = \Omega_c \mathbf{D}^{c} \dot{\boldsymbol{\varepsilon}}^{c} + \Omega_s \mathbf{D}^{s} \dot{\boldsymbol{\varepsilon}}^{s} \tag{4}$$

where $\mathbf{D}^{\text{eq}}$ = material stiffness matrix of the equivalent material; and $\mathbf{D}^{c}$ and $\mathbf{D}^{s}$ = material stiffness matrices of the column and soil, respectively.

To use the aforementioned homogenization equations in a useful manner, one needs to introduce local mechanical balance assumptions and kinematic constraints that suit the problem to be tackled. Because this paper focuses on the deep-mixed column used to improve the soil under embankments, it is assumed that the columns and the soil will be deforming equally in the vertical direction, with perfect bonding at the column–soil interface. The perfect bonding in this case eliminates the need for a special interface element at the column–soil interface. Considering y to be the vertical axis, these assumptions can be met mathematically by satisfying the following conditions:

Kinematic constraints (equal vertical deformation and shearing in the out-of-plane direction):

$$\dot{\varepsilon}_{yy}^{\text{eq}} = \dot{\varepsilon}_{yy}^{c} = \dot{\varepsilon}_{yy}^{s} \text{ and } \dot{\gamma}_{xz}^{\text{eq}} = \dot{\gamma}_{xz}^{c} = \dot{\gamma}_{xz}^{s}$$

Local mechanical balance (perfect bonding with a continuous stress field):

$$\dot{\sigma}_{xx}^{\text{eq}} = \dot{\sigma}_{xx}^{c} = \dot{\sigma}_{xx}^{s}; \quad \dot{\sigma}_{zz}^{eq} = \dot{\sigma}_{zz}^{c} = \dot{\sigma}_{zz}^{s}$$
$$\dot{\sigma}_{xy}^{\text{eq}} = \dot{\sigma}_{xy}^{c} = \dot{\sigma}_{xy}^{s}; \quad \dot{\sigma}_{zy}^{eq} = \dot{\sigma}_{zy}^{c} = \dot{\sigma}_{zy}^{s} \tag{5}$$

After mathematical manipulation using Eqs. (1) and (3)–(5), the following analytic form for $\mathbf{D}^{\text{eq}}$ can be derived (Lee and Pande 1998):

$$\mathbf{D}^{\text{eq}} = \Omega_c \mathbf{D}^{c} \mathbf{S}^{c} + \Omega_s \mathbf{D}^{s} \mathbf{S}^{s} \tag{6}$$

where $\mathbf{S}^{c}$ and $\mathbf{S}^{s}$ = so-called strain distribution matrices that are dependent on the constituent stiffness matrices (i.e., $\mathbf{D}^{c}$ and $\mathbf{D}^{s}$) and volume fractions (i.e., Ω_c and Ω_s). The strain distribution matrices are used to estimate the ratio of column and soil strain increment to the total equivalent strain increment. The mathematical derivation of $\mathbf{D}^{\text{eq}}$, $\mathbf{S}^{c}$, and $\mathbf{S}^{s}$ is out of the scope of the current study; however, the interested reader is referred to Lee and Pande (1998) and Vogler (2008) for complete details.

Numerical Implementation

The homogenization procedure is implemented into the commercial finite-element code PLAXIS 2D (version 2024) as a user-defined model based on Vogler (2008). The main steps followed by the scheme are clarified in the flowchart in Fig. 3. In the first step, assuming elastic behavior for columns and soil, the equivalent elastic material stiffness matrix $\mathbf{D}^{\text{eq}}$ is formed analytically employing Eq. (6). Then, following the standard finite-element procedure, the global stiffness matrix $\mathbf{K}$ is assembled and the equivalent displacement increment $\Delta \boldsymbol{u}_{\text{eq}}$ is calculated in response to the applied external force increment $\Delta \mathbf{F}$. Consequently, the equivalent strain increment $\Delta \boldsymbol{\varepsilon}^{\text{eq}}$ is estimated at Gauss (stress integration) points through the gradients of shape functions stored in the matrix $\mathbf{B}$. At this point, the strain distribution matrices $\mathbf{S}^{c,s}$ are used to distribute the equivalent strain increment $\Delta \boldsymbol{\varepsilon}^{\text{eq}}$ into soil strain increment $\Delta \boldsymbol{\varepsilon}^{s}$ and column strain increment $\Delta \boldsymbol{\varepsilon}^{c}$ according to

$$\Delta \boldsymbol{\varepsilon}^{c} = \mathbf{S}^{c} \Delta \boldsymbol{\varepsilon}^{\text{eq}}; \; \Delta \boldsymbol{\varepsilon}^{s} = \mathbf{S}^{s} \Delta \boldsymbol{\varepsilon}^{\text{eq}} \tag{7}$$

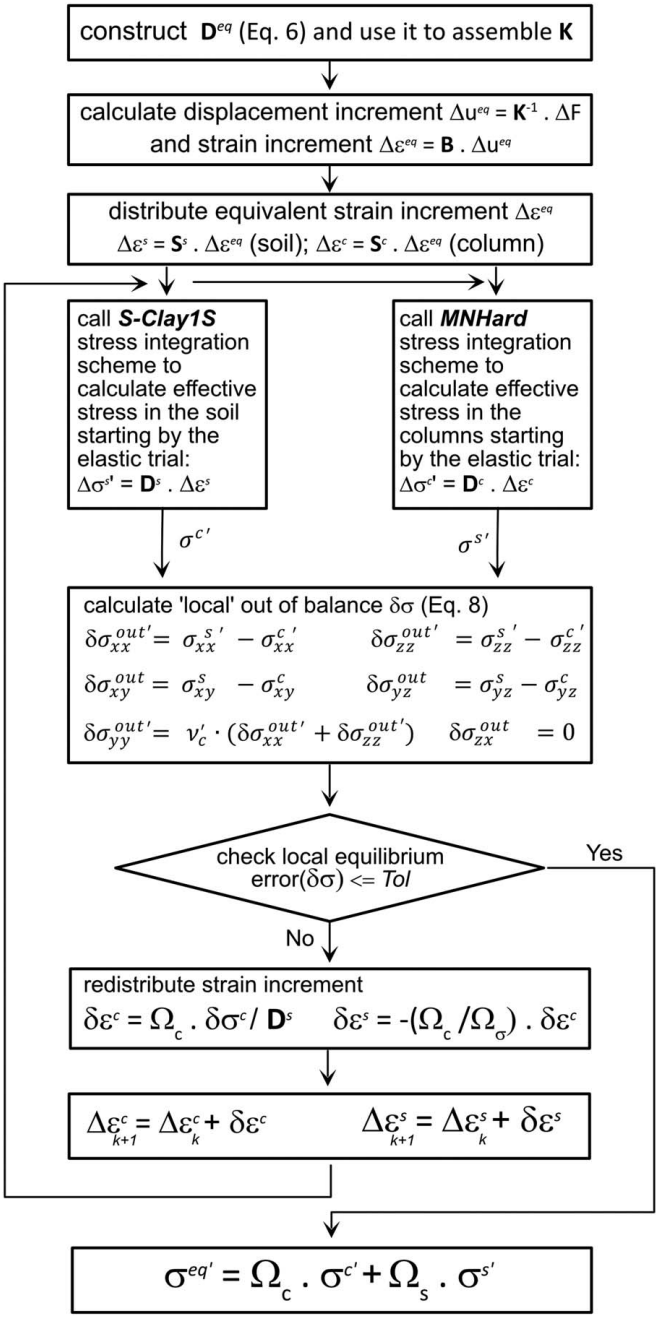

Fig. 3. Main steps followed by the homogenization routine.

Afterward, any suitable stress–strain relationship (constitutive model) can be used for stress integration (i.e., to calculate the corresponding increment of effective stresses in the soil $\Delta\boldsymbol{\sigma}^{c'}$ and the column $\Delta\boldsymbol{\sigma}^{s'}$ separately). In this study, the SClay1S model (Koskinen et al. 2002; Wheeler et al. 2003; Karstunen et al. 2005, 2006) is used to model the natural clay behavior, whereas the Matsuoka–Nakai hardening (MNHard) model (Benz 2007) is employed to capture the behavior of the mixed columns. Both models are introduced in the "On the Used Constitutive Models" section. For numerical stress integration, MNHard and SClay1S can be implemented using any suitable explicit (Sloan et al. 2001) or implicit (Borja and Lee 1990; De Borst and Heeres 2002; Abed 2008) scheme. In the current study, within the VAT user-defined model, an implicit scheme is used, enhanced by a subincrementation procedure to avoid excessive strain increments that might lead to numerical difficulties. Having estimated the effective stress increment in each component (i.e., soil and column), the corresponding final effective stresses (i.e., $\boldsymbol{\sigma}^{c'}$ and $\boldsymbol{\sigma}^{s'}$) are subjected to the local balance check provided by Eq. (5). If the conditions are satisfied, then the final effective stresses in the equivalent material $\boldsymbol{\sigma}^{eq'}$ are estimated based on Eq. (1); otherwise, a strain redistribution procedure is initiated and iteratively repeated until the local balance is satisfied. This redistribution procedure is discussed in the following paragraph.

Iterative Procedure for Local Mechanical Balance

To assess the local balance assumption as provided by Eq. (5), the local out of balance $\delta\sigma^{out'}$ is estimated for each stress component as follows:

$$\begin{aligned}
&\delta\sigma_{xx}^{out'} = \sigma_{xx}^{s'} - \sigma_{xx}^{c'};\ \delta\sigma_{zz}^{out'} = \sigma_{zz}^{s'} - \sigma_{zz}^{c'}\\
&\delta\sigma_{xy}^{out} = \sigma_{xy}^{s} - \sigma_{xy}^{c};\ \delta\sigma_{yz}^{out} = \sigma_{yz}^{s} - \sigma_{yz}^{c}\\
&\delta\sigma_{yy}^{out'} = \nu_c' \cdot (\delta\sigma_{xx}^{out'} + \delta\sigma_{zz}^{out'});\ \delta\sigma_{zx}^{out} = 0
\end{aligned} \tag{8}$$

Then, the relative error (RE) measure $err_{ij} = \delta\sigma_{ij}^{out'} / \sigma_{ij}^{s'} \le Tol$ is used to determine the occurred error for each stress component. This check excludes $\delta\sigma_{yy}^{out'}$ and $\delta\sigma_{zx}^{out}$ because they are imposed and calculated based on other out-of-balance components. A tight relative error tolerance $Tol = 10^{-8}$ is used in this study, which can be loosened depending on the user's judgment or in the case of numerical issues with convergence. If one of the stress components violates the local balance, a redistribution of strain increments is carried out as follows:

$$\delta\boldsymbol{\varepsilon}^{c} = \Omega_c \cdot \mathbf{D}^{c-1} \cdot \delta\boldsymbol{\sigma}^{out'} \tag{9}$$

where $\boldsymbol{\delta\varepsilon^{c}}$ = strain correction to be distributed to the column strain increment $\boldsymbol{\Delta\varepsilon^{c}}$. To estimate the strain correction $\boldsymbol{\delta\varepsilon^{s}}$ to be distributed to the soil strain increment $\boldsymbol{\Delta\varepsilon^{s}}$, the equivalent strain increment imposed by the finite-element calculations should stay the same with $\boldsymbol{\delta\varepsilon^{eq}} = 0$; thus,

$$\delta\boldsymbol{\varepsilon}^{eq} = \Omega_c \cdot \delta\boldsymbol{\varepsilon}^{c} + \Omega_s \cdot \delta\boldsymbol{\varepsilon}^{s} = 0 \overset{\text{using Eq. (9)}}{\rightarrow} \Delta\boldsymbol{\varepsilon}^{s} = -\frac{\Omega_c}{\Omega_s} \cdot \delta\boldsymbol{\varepsilon}^{c} \tag{10}$$

Finally, the new corrected strain increments can be estimated as

$$\Delta\boldsymbol{\varepsilon}_{k+1}^{c} = \Delta\boldsymbol{\varepsilon}_{k}^{c} + \delta\boldsymbol{\varepsilon}^{c};\Delta\boldsymbol{\varepsilon}_{k+1}^{s} = \Delta\boldsymbol{\varepsilon}_{k}^{s} + \delta\boldsymbol{\varepsilon}^{s} \tag{11}$$

to be used in the next $k+1$ stress correction iteration. The calculations in Eqs. (8)–(11) are repeated until the local balance is satisfied with $err_{ij} \le Tol$ (see Fig. 3 for clarification).

On the Used Constitutive Models

SClay1S soil model

The natural clay is modeled using SClay1S (Koskinen et al. 2002; Karstunen et al. 2005), which is an associated elastoplastic critical state type of model. It captures the main features of natural clay behavior, such as anisotropy and destructuration. Nonetheless, for simplicity, SClay1S assumes an isotropic elasticity, which requires, similar to the modified Cam-clay (MCC) (Schofield and Wroth 1968; Wood 1990), a constant effective Poisson's ratio ν' (or elastic shear modulus G) and the unloading–reloading (swelling) index κ to reproduce the elastic behavior. The plastic behavior is controlled by a rotated and sheared yield surface for the intact clay (Fig. 4). For the simplified triaxial stress state, the yield criterion can be

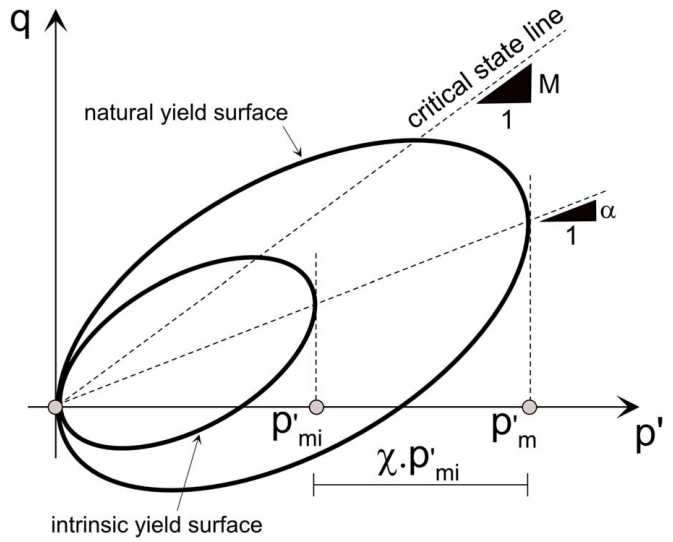

Fig. 4. SClay1S yield surfaces in triaxial stress space.

written as

$$f = (q - \alpha \cdot p')^2 - (M^2 - \alpha^2) \cdot (p'_m - p') \cdot p' \tag{12}$$

where q, p', and M = deviatoric stress, isotropic effective stress, and stress ratio $\eta = q/p'$ at the critical state, respectively. Parameter p'_m defines the size of the yield surface. Parameter α is a measure of the current anisotropy and defines the inclination of the yield surface. SClay1S also defines the so-called intrinsic yield surface, which has the same mathematical formulation as the natural yield surface in Eq. (12); however, its size is defined by the intrinsic preconsolidation p'_{mi}, which relates to p'_m through the bonding parameter χ as follows (Gens and Nova 1993):

$$p'_m = (1 + \chi) \cdot p'_{mi} \tag{13}$$

The mathematical formulation of SClay1S comprises three hardening mechanisms:

1. A rotational hardening that controls the evolution of anisotropy with stress variation: The induced incremental rotation of the yield surface $d\alpha$ is solely controlled by the plastic strain increment $d\varepsilon^p$ with different contributions of its components, namely, the positive compressive increment of plastic volumetric strain being captured by Macaulay brackets $d\varepsilon^p_v$ and the absolute value of the increment of plastic deviatoric strain $|d\varepsilon^p_d|$. The rotational hardening rule can be written under triaxial stress conditions as

$$d\alpha = \omega \cdot \left[\left(\frac{3\eta}{4} - \alpha \right) \cdot \langle d\varepsilon^p_v \rangle + \omega_d \cdot \left(\frac{\eta}{3} - \alpha \right) \cdot |d\varepsilon^p_d| \right] \tag{14}$$

   where ω and ω_d = model parameters that control the absolute and relative effectiveness of volumetric and deviatoric plastic strain increments in rotating the yield surface (i.e., destroying the anisotropy), respectively.
2. A volumetric hardening that controls the intrinsic yield surface size: Similar to MCC and corresponding to the name, this hardening rule assumed the size to be only a function of the volumetric component of the plastic strain increment and given as

$$d\,p'_{mi} = \frac{(1 + e_o) \cdot p'_{mi} \cdot d\varepsilon^p_v}{\lambda_i - \kappa} \tag{15}$$

   where $d\,p'_{mi}$ = increment in the intrinsic effective preconsolidation pressure; e_o = initial void ratio; and λ_i = intrinsic compression index being estimated using the results of an isotropic compression test or an oedometer test on a reconstituted sample. Note that any change in the size of the intrinsic yield surface will be reflected as a change in the size of the natural yield surface because they are coupled through Eq. (13).
3. A destructuration that rules the degradation of bonds: Again, the debonding increment $d\chi$ is a function of the plastic strain increment only, with different contributions of the absolute value of its components $d\varepsilon^p_v$ and $d\varepsilon^p_d$, which can be written as

$$d\chi = -\xi \cdot \chi \cdot [|d\varepsilon^p_v| + \xi_d \cdot |d\varepsilon^p_d|] \tag{16}$$

   where ξ and ξ_d = model parameters that control the absolute and relative effectiveness of volumetric and deviatoric plastic strain increments in destroying the bonding, respectively.

The generalization of the model into the three-dimensional stress space can be found in several references, e.g., Wheeler et al. (2003) and Karstunen et al. (2005), among many others.

In total, the model requires, besides the normal MCC parameters (ν', κ, λ_i, M, e_o, and p'_{mo}), six additional parameters: three to describe the anisotropic behavior (ω, ω_d, and α_o) and three to describe the bond degradation (ξ, ξ_d, and χ_o). These extra parameters can be estimated based on the results of triaxial tests on natural samples. For instance, parameter ω_d can be determined from the stress ratio at critical state following the procedure described in Wheeler et al. (1999, 2003). ω in turn can be calibrated by simulating undrained shearing in triaxial extension (Gras et al. 2018). While ξ and ξ_d can be estimated based on an optimization procedure as described by Koskinen et al. (2002), which requires drained triaxial testing, they can also be estimated by simulating the oedometric stress–strain curve. The study by Gras et al. (2018) also provides guidance on estimating these parameters in the case of the absence of experimental data. Table 1 summarizes the required tests to derive SClay1S parameters.

In this study, given that the clay is only lightly overconsolidated, the initial inclination of the yield surface α_o was estimated based on the K_o^{NC} value following Jaky's formula ($K_o^{NC} = 1 - \sin\varphi'$) with $\alpha_o = (\eta^2_{K_o^{NC}} + 3\eta_{K_o^{NC}} - M^2)/3$, while the empirical formula $\chi_o = S_t - 1$ suggested by Koskinen et al.(2002) was employed to estimate the initial bonding as a function of clay sensitivity S_t. Table 3 lists the value of SClay1S parameters derived for Paimio clay in Finland to be used later in the numerical application.

Table 1. SClay1S model parameters and the required tests to derive them

Method of derivation	Definition
Fall cone test	Initial amount of bonding, χ_0
Oedometer test	Modified swelling index, $\kappa^* = \frac{\kappa}{(1+e_0)}$
	Modified intrinsic compression index, $\lambda^* = \frac{\lambda_i}{(1+e_0)}$
	Poisson's ratio, ν'
	Preoverburden pressure (POP) or overconsolidation ratio (OCR)
Undrained triaxial tests	Stress ratio at the critical state in triaxial compression, M
	Relative rate of rational hardening due to deviatoric strain, ω_d
	Initial value of anisotropy, α_0
Model calibration	Absolute rate of rotational hardening, ω
	Absolute rate of destructuration, ξ
	Relative rate of destructuration due to deviatoric strain, ξ_d

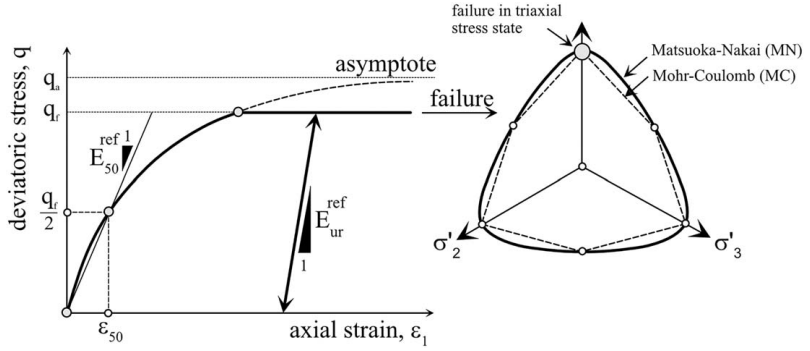

Fig. 5. Hyperbolic stress–strain relationship for the shearing phase of a standard drained triaxial test at a confining pressure of $\sigma'_3 = p_{\text{ref}}$. In the MNHard model, the failure is captured by the Matsuoka–Nakai (MN) criterion [shown in the π-plane together with the Mohr–Coulomb (MC) criterion for comparison].

MNHard Material Model

Based on limited drained triaxial test results on cement-mixed clay provided by Aalto (2003), one notices that adding a binder (cement in this case) to a normally or slightly overconsolidated soft clay alters its mechanical behavior from being mainly density dependent (volumetric hardening) to a typical coarse grained material response that is controlled by frictional (shear) hardening. Therefore, the so-called MNHard model (Matsuoka and Nakai 1982; Benz 2007) was adopted to capture the behavior of mixed columns. MNHard is a purely shear hardening elastoplastic model, where the plastic strains occur due to primary deviatoric loading with Matsuoka–Nakai (MN) as a failure criterion. No volumetric hardening is considered in the model. The following paragraphs discuss in more detail the model response during loading and unloading, plasticity, and shear failure.

MNHard during Loading and Unloading. The model assumes nonlinear elasticity based on the hyperbolic stress–strain relationship by Kondner and Zelasko (1963) and its later modification by Duncan and Chang (1970). Both E'_{50} and E'_{ur} (Fig. 5) are dependent on the effective confining pressure σ'_3 following the equations

$$E'_{50} = E'^{\text{ref}}_{50}\left(\frac{\sigma'_3 + a}{p_{\text{ref}} + a}\right)^m; \quad E'_{ur} = E'^{\text{ref}}_{ur}\left(\frac{\sigma'_3 + a}{p_{\text{ref}} + a}\right)^m \tag{17}$$

where E'^{ref}_{50} and E'^{ref}_{ur} = reference secant and unloading–reloading elastic modulus at a reference effective confining pressure p_{ref}, respectively. The auxiliary term $a = c' \cdot \cot\varphi'$ and the power m controls the stiffness stress dependency with typical values ranging between $m = 0.5$ for sand and $m = 1.0$ for clay. Note that the values of the effective shear resistance parameters c' and φ' play a role in these formulae, which will be pronounced in cohesive materials.

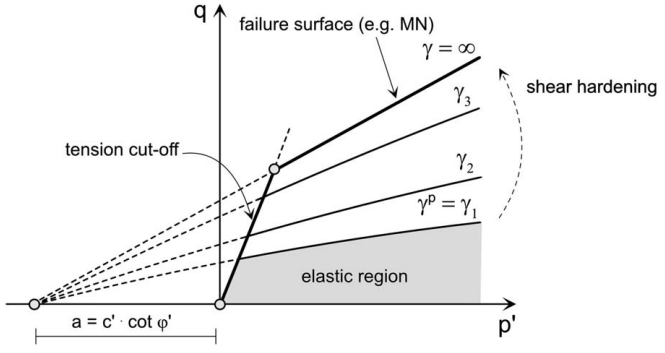

Fig. 6. Evolution of shear yield surfaces in the p'–q plane with increasing plastic shear strain, capturing shear hardening relevant to deep-mixed columns as a frictional material.

Fig. 5 illustrates the definition of the elastic moduli using the $q-\varepsilon_1$ stress–strain curve for the shearing phase of a standard drained triaxial test. In fact, such a curve can be used to calibrate the model parameters (e.g., E'^{ref}_{50}, E'^{ref}_{ur}, m, p_{ref}, φ', and c').

MNHard in Plasticity. According to MNHard formulation, plastic strain occurs due to primary deviatoric loading only pushing the shear yield surface gradually toward the limiting shear failure surface (Fig. 6). Considering the Matsuoka–Nakai criterion (Matsuoka and Nakai 1982) as the limiting shear failure criterion, the shear yield criterion is defined as

$$f^s = \frac{I^a_1 I^a_2}{I^a_3} - \frac{9 - \sin^2\varphi'_m}{1 - \sin^2\varphi'_m} \tag{18}$$

where I^a_1, I^a_2, and I^a_3 = first, second, and third modified stress invariants, respectively, which are defined as

$$I^a_1 = \sigma^a_1 + \sigma^a_2 + \sigma^a_3; \quad I^a_2 = \sigma^a_1 \cdot \sigma^a_2 + \sigma^a_2 \cdot \sigma^a_3 + \sigma^a_3 \cdot \sigma^a_1; \quad I^a_3 = \sigma^a_1 \cdot \sigma^a_2 \cdot \sigma^a_3 \tag{19}$$

with $\sigma^a_i = \sigma'_i + a$: $i = 1, 2, 3$.

The mobilized shear strength angle φ'_m is estimated based on the accumulated plastic shear strain γ^p according to the following formula:

$$\sin\varphi' m = \sin\varphi' \cdot \frac{\gamma^p}{\gamma_a + \gamma^p} : \gamma_a = \gamma_{50} \cdot (1 - \sin\varphi') \text{ and } \gamma_{50} \approx \frac{3}{2} \cdot \varepsilon_{50} = \frac{3}{4} \cdot \frac{q_a}{E_{50}} \tag{20}$$

In the model, the asymptotic shear strength q_a is cut off to a threshold failure value $q_f = R_f \cdot q_a$, where R_f is taken as 0.9 in most cases.

It is assumed in the formulation of the model that the elastic part of the shear strain is negligibly small and, thus, the plastic part can be considered equal to the total shear strain, being given as

$$\gamma^p \approx \gamma = \frac{1}{\sqrt{2}} \cdot \sqrt{(\varepsilon_1 - \varepsilon_2)^2 + (\varepsilon_2 - \varepsilon_3)^2 + (\varepsilon_3 - \varepsilon_1)^2} \tag{21}$$

During elasticity, the value of φ'_m remains constant because no plastic shear strain γ^p occurs. The yield loci defined by Eq. (18) expand with the increase of the accumulated γ^p, where each locus represents a constant plastic shear strain surface in stress space (Fig. 6).

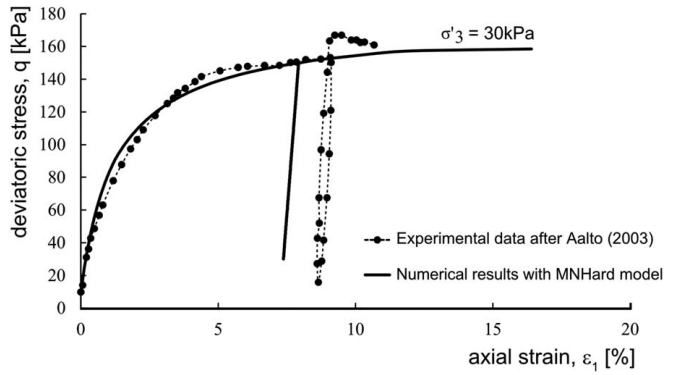

Fig. 7. MNHard numerical results calibrated against the drained triaxial test result of a cement-mixed under a confining pressure $\sigma'_3 = 30$ kPa.

Finally, MNHard is a nonassociated model assuming Drucker–Prager-like plastic potential g (Drucker and Prager 1952)

$$g = \frac{6 \cdot \sin\psi'_m}{3 - \sin\psi'_m} \cdot (p' + c' \cdot \cot\varphi') \tag{22}$$

The mobilized dilatancy angle ψ'_m is estimated based on Rowe (1962) as

$$\sin\psi'_m = \frac{\sin\varphi'_m - \sin\varphi'_{cv}}{1 - \sin\varphi'_m \cdot \sin\varphi'_{cv}} \tag{23}$$

where the internal friction angle at the critical state φ'_{cv} is derived based on the dilatancy angle ψ' as follows:

$$\sin\varphi'_{cv} = \frac{\sin\varphi' - \sin\psi'}{1 - \sin\varphi' \cdot \sin\psi'} \tag{24}$$

Failure Criterion in MNHard. The shear yield surface defined in the previous paragraph expands with increasing γ^p until hitting a limiting maximum failure surface. This happens when the mobilized shear resistance angle φ'_m reaches the maximum available internal friction angle φ' and the shear yield surface becomes the MN shear failure surface, defined as

$$f^{\mathrm{MN}} = \frac{I_1^a I_2^a}{I_3^a} - \frac{9 - \sin^2\varphi'}{1 - \sin^2\varphi'} \tag{25}$$

The shape of the MN failure surface in the deviatoric plane (π-plane) is shown in Fig. 5 together with the well-known Mohr–Coulomb (MC) failure surface. As can be noticed, MN and MC predict the same shear resistance in triaxial compression and extension, while MN predicts slightly higher resistance under other stress paths (e.g., plane-strain conditions). MN was chosen in this study because there is experimental evidence showing that MN is more realistic than MC (Matsuoka and Nakai 1982). In addition, the smoothness of the mathematical formulation of MN is appealing from a numerical implementation point of view, compared to MC, which suffers singularities at the intersections between different failure planes.

For this study, the drained triaxial tests provided by Aalto (2003) for cement-mixed soil samples were used to derive the MNHard model parameters that will be used in the numerical application discussed later. Fig. 7 shows an example of the test results under a confining pressure σ_3 of 30 kPa and the calibrated numerical results based on the MNHard model, which yielded the parameters listed in Table 2.

Verification and Validation

The results of the implemented VAT user-defined model were first verified against the numerical results of full 3D analyses and then validated against experimental results of Paimio trial embankments in Finland provided by Vepsäläinen and Arkima (1992). The following section provides a general description of the trial embankments and the construction site in terms of geometry, stratigraphy, and material properties before discussing the numerical model.

Trial Embankments and Construction Site in Paimio

To study the arching in road embankments, the Finnish Road Administration constructed four trial embankments between 1989 and 1991 in the region of Paimio, located at about 30 km east of Turku in Finland (Vepsäläinen and Arkima 1992). The embankments were made of slightly compacted sand with an average unit weight of $\gamma = 18.5$ kN/m^3. One of these embankments was constructed on greenfield conditions (natural virgin soil without any improvement). The other three were constructed on an improved soil with deep-mixed columns using cement as a binder with different column center-to-center (c/c) distances, namely, 1.0, 1.2, and 1.4 m. The thickness of the soft clay at the test site varies between 8 and 13 m. The desiccated dry crust at the top is about 1–2 m thick. Based on the in situ vane shear tests, the average undrained shear strength of the soft clay layer underneath is in the range 10 kN/m^2 just under the cry crust, increasing with depth. The modified Cam-clay model parameters of the clay layers were derived by Vepsäläinen et al. (1991) and Vepsäläinen and Arkima (1992) based on one-dimensional (1D) compression tests and triaxial tests conducted at Helsinki University of Technology (currently, Aalto University). Several tests were also carried out to estimate the index and physical properties of the clay (Fig. 8).

Fig. 9 is modified after Vepsäläinen and Arkima (1992) and shows a top view of the embankments and a cross section through the embankment on natural clay and the one supported by mixed columns with $c/c = 1.0$ m. The average diameter of the deep-mixed column is 0.6 m. As can be seen in Fig. 9(b), the depth of the columns is not constant but varies with the stratigraphy following the top surface of the stiffer stratum at the bottom of the clay layer. The height of the embankments is also slightly varying, which was important to consider in the modeling.

The field measurements showed that the groundwater table fluctuated at a depth of 2.0–3.0 m over the time the test embankments were monitored; however, in this study, the groundwater table was kept constant at an average depth of 2.7 m.

The embankments were heavily instrumented so that the most relevant variables (e.g., displacements, pore-water pressure, earth pressures in soil and columns, etc.) were recorded for 2 years (1989–1991). Fig. 10 shows an example of the used instrumentation in the case of the embankment on natural clay. The

Table 2. MNHard model parameters calibrated against the drained triaxial test result

γ_{sat} (kN/m^3)	E_{50}^{ref} (kN/m^2)	E_{ur}^{ref} (kN/m^2)	p'_{ref} (kN/m^2)	ν' (—)	m (—)	φ' (degrees)	c' (kN/m^2)	ψ' (degrees)
13.8	12,000	27,000	100.0	0.35	0.7	37	14	0

Source: Data from Aalto (2003).

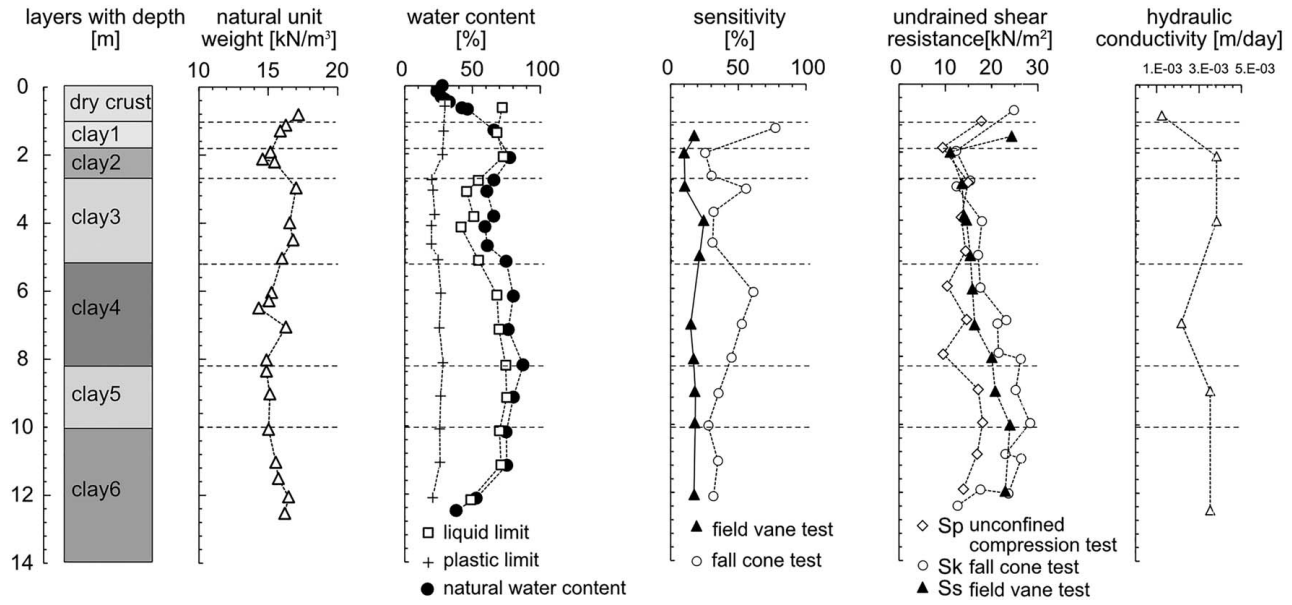

Fig. 8. Soil profile at the location of Paimio trial embankments.

instrumentation included settlement plates and a magnetic extensometer to measure deformations, open and closed piezometers for pore-water pressure measurements, and settlement observation points for monitoring the surface settlement. The vertical and horizontal pressures under the embankments were also measured using pressure cells. The interested reader can find the full set of experimental measurements in Vepsäläinen and Arkima (1992).

Finite-Element Calculations

Trial Embankment on Greenfield

Fig. 11 presents the geometry and the finite-element mesh used to simulate the trial embankment on greenfield. Due to symmetry, only one half of the embankment was modeled, assuming plane-strain conditions. The latter was assumed, despite the embankment being square, to enable comparisons with the embankment with

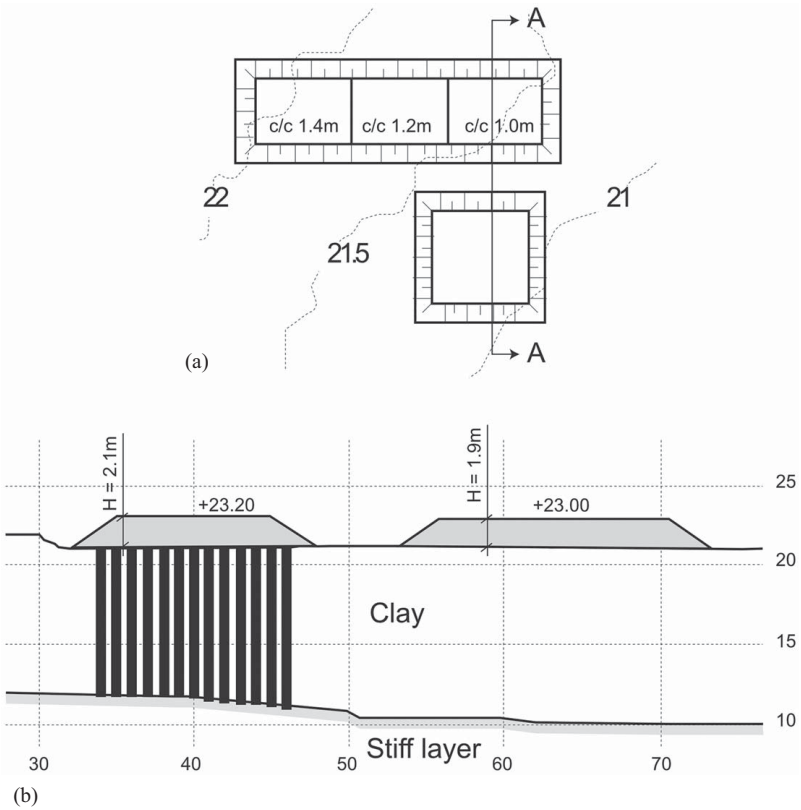

Fig. 9. Trial embankments' geometry: (a) top view; and (b) cross section A–A. (Adapted from Vepsäläinen and Arkima 1992.)

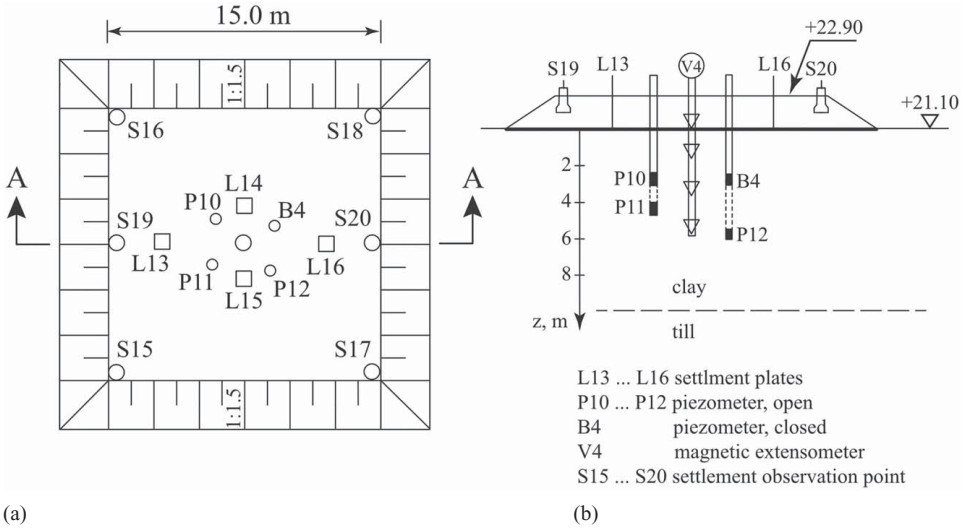

Fig. 10. Instrumentations in the case of the trial embankment on the natural untreated Paimio clay: (a) top view; and (b) cross section A–A. ("The trial embankments in Vaasa and Paimio, Finland," P. Vepsäläinen, O. Arkima, M. Lojander, A. Näätänen, Xth European Conference on Soil Mechanics and Foundation Engineering, © 1991, reprinted by permission of Taylor & Francis Ltd., http://tandfonline.com.)

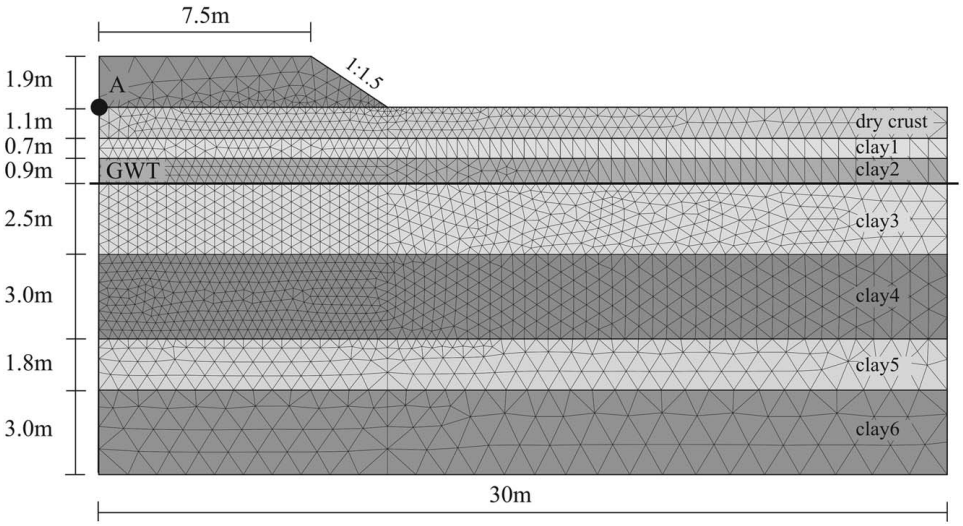

Fig. 11. FE model for the trial embankment on natural clay.

deep-mixed columns. In fact, the analysis was repeated assuming axisymmetric conditions—after adjusting the embankment dimensions to transfer the same external load to the natural clay. The small difference in the results, as it is clear in Fig. 12, confirms the appropriateness of the plane-strain conditions.

The mesh comprises 3,561 15-noded elements with 12 stress integration points per element. The clay layers are modeled as SClay1S material with parameters listed in Table 3. Many of these parameters (i.e., the modified Cam-clay parameters) are adopted directly from the original report by Vepsäläinen and Arkima (1992). The extra parameters for anisotropy and bonding are calibrated using the procedures suggested by Koskinen et al. (2002) and Wheeler et al. (2003) as well as against the provided field measurements. The in situ earth pressure coefficient was estimated based on the formula

$$K_o^{\mathrm{OCR}} = K_o^{\mathrm{NC}} \mathrm{OCR}^{\sin\varphi'} \text{ with } K_o^{\mathrm{NC}} = 1 - \sin\varphi' \tag{26}$$

As for the calculation phases, first, the initial stresses were generated based on the K0 procedure, followed by a plastic nil step, and then the embankment was constructed, followed by a consolidation analysis for 800 days (a little over 2 years) with an open hydraulic boundary condition at the bottom of the clay layer. The calculated vertical displacements were monitored at Point A shown on Fig. 11, while the pore-water pressure was recorded at depths 3, 4.5, and 6 m under the embankment centerline corresponding to the location of in situ measurements.

In Fig. 12, the calculated vertical displacements at Point A are plotted against the measured data. The figure also shows the percentage of relative error in calculations, defined as $\mathrm{RE} = 100 \times |(u_m - u_{\mathrm{FE}})/u_m|$, where u_m is the measured quantity (i.e., vertical displacement in this case) and u_{FE} is the corresponding finite-element prediction. Apart from the initial deviation, the overall match can be considered excellent, with an average relative error of 3%, and the clay behavior is replicated well by the SClay1S model.

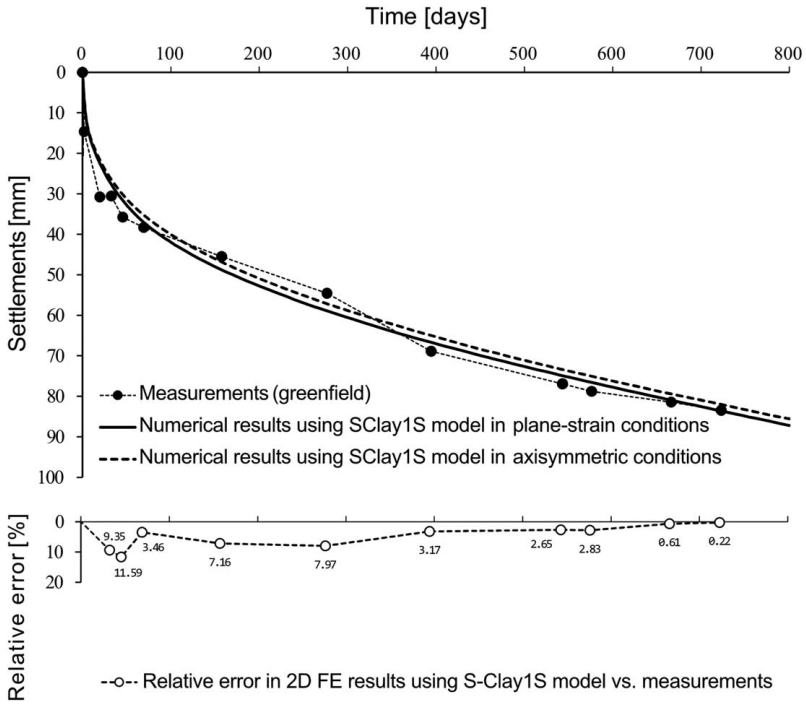

Fig. 12. Calculated vertical displacement and relative error at Point A compared to in situ measurements for an embankment on greenfield.

Table 3. Calibrated SClay1S parameters for Paimio clay

Layer	γ_{sat} (kN/m^3)	e_0	κ^*	ν	λ^*	M	ω	ω_d	ξ	ξ_d	OCR	α_0	χ_0	$k_x = k_y$ (m/day)	K_o^{NC}	K_o^{OCR}
Dry crust	16.2	1.8	0.007	0.1	0.075	1.1	0	0	0	0	4	0	0	1.22×10^{-5}	0.53	1.0
Clay1	16.2	1.8	0.007	0.1	0.075	1.1	60	0.554	5	0.2	4	0.436	3	1.22×10^{-5}	0.53	1.0
Clay2	15.0	2.1	0.016	0.1	0.17	1.1	40	0.554	5	0.2	2	0.436	3	5.1×10^{-5}	0.53	0.73
Clay3	16.0	1.9	0.005	0.1	0.137	1.1	40	0.554	5	0.2	1.15	0.436	9	5.1×10^{-5}	0.53	0.56
Clay4	15.0	2.15	0.0158	0.1	0.285	1.2	25	0.76	5	0.2	1.4	0.457	9	2.07×10^{-5}	0.5	0.59
Clay5	15.5	2.5	0.014	0.1	0.23	1.1	25	0.55	5	0.2	1.15	0.436	9	3.53×10^{-5}	0.53	0.56
Clay6	16.2	1.9	0.014	0.1	0.207	1.1	35	0.55	5	0.2	1.2	0.435	7	3.53×10^{-5}	0.53	0.57

This analysis gives confidence about the adopted model parameters, which will be used as part of the input for the VAT model when simulating the behavior of the trial embankments on improved soil.

The model also performed well in replicating the measured total pore-water pressure (excess + hydrostatic) as depicted in Fig. 13. The deviation at 6 m depth that happened after Day 200 might be related to the massive piling activities that took place during the

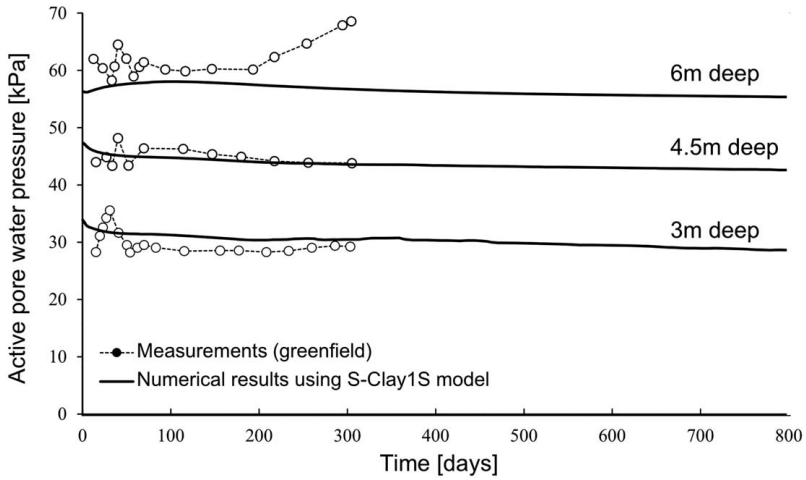

Fig. 13. Calculated pore-water pressure versus measured values at different depths under the embankment centerline for the case of embankment on greenfield.

Int. J. Geomech., 2026, 26(1): 04025322

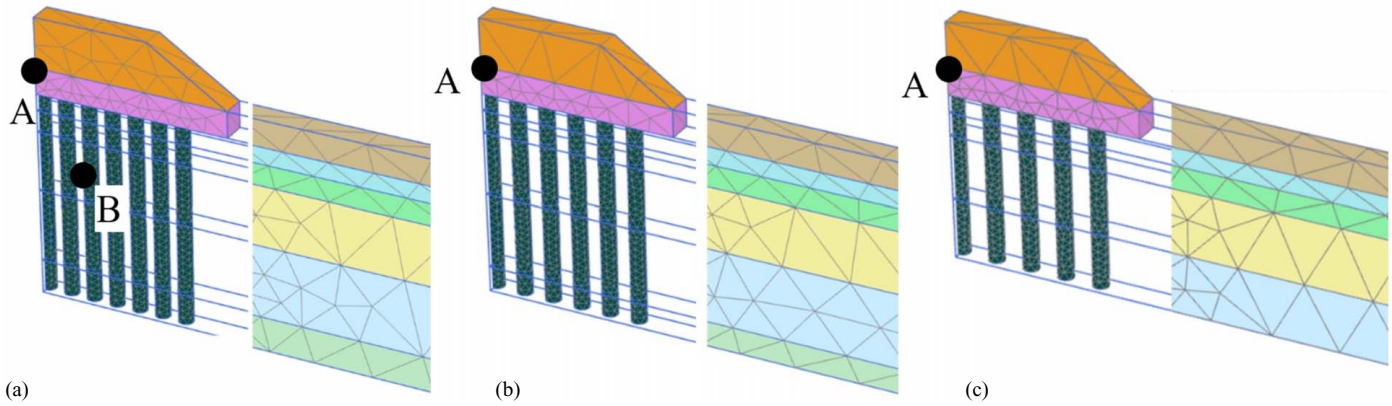

Fig. 14. 3D FE model for the trial embankments supported by a deep-mixed column with different c/c spacings (m): (a) 1.0; (b) 1.2; and (c) 1.4.

Table 4. Clarification of the geometry variation in the trial embankments on a deep-mixed column with different c/c spacings

c/c (m)	Column volume fraction Ω_c (—)	Embankment height (m)	Embankment width at the top (m)	Average column height (m)	3D strip width (m)
1.0	0.283	2.1	9.6	9.6	1.0
1.2	0.196	1.9	10.0	9.2	1.2
1.4	0.144	1.7	10.0	7.5	1.4

construction of the actual motorway next to the testing site and caused disturbance and a sudden increase in the excess pore-water pressure (Bredenberg et al. 1999).

Trial Embankments on Improved Soil

Each trial embankment on deep-mixed columns was modeled in two different ways: first, as a full 3D problem and, second, as a 2D plane-strain model using the VAT. As such, the 3D results serve as a verification tool for the VAT, while the in situ measurements will be used to validate the method.

Full 3D FE Model

Fig. 14 illustrates the geometry and the 3D finite-element meshes as used to model the different trial embankments with $c/c = 1$, 1.2, and 1.4 m. The mesh was generated using 10-node tetrahedral finite elements with four stress integration points per element. Due to symmetry, it is enough to model one strip of the embankment with one row of deep-mixed columns. As can be noticed, there are slight differences in the total heights of the embankments, the average length of the columns, and the number of columns depending on the spacing. Table 4 lists the differences in geometry among the embankments to be considered when generating the FE model.

In the 3D analyses, the deep-mixed columns were modeled as individual volume elements, assumed to behave according to the MNHard model with the model parameters listed in Table 2. The clay layers were assigned the SClay1S model with the corresponding parameters in Table 3. The part of the dry crust under the embankments on improved soil was assigned higher stiffness parameters ($\kappa = 0.005$ and $\lambda = 0.05$) to account for the effect of partial improvement of this layer. The columns were simulated as wish-in-place with no installation effect on the initial stresses and/or state. Thus, after generating the initial stresses, the columns were assigned with an MNHard material model, and then the embankments were constructed, followed by 2 years of consolidation. The results were monitored at Points A and B, as shown in Fig. 14.

2D FE Model Using the VAT

For the 2D model, a similar setup to the case of greenfield in the "Trial Embankment on Greenfield" section is used here in terms of soil layers and parameters; however, the region of improved clay is replaced by the VAT material. Fig. 15 presents the 2D finite-element mesh used in the case of $c/c = 1.0$ m.

In addition to the SClay1S parameters listed in Table 3, the VAT user-defined model requires the parameters, as listed in Table 2, for the MNHard model to simulate the deep-mixed cement columns. On top of that, the VAT requires the input of the column volume fraction Ω_c. Because we have a regular rectangular pattern, based

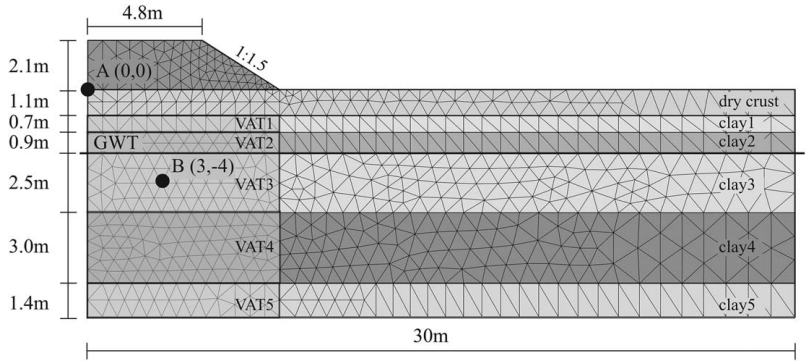

Fig. 15. FE model using the VAT to simulate the trial embankment on a deep-mixed column with $c/c = 1.0$ m.

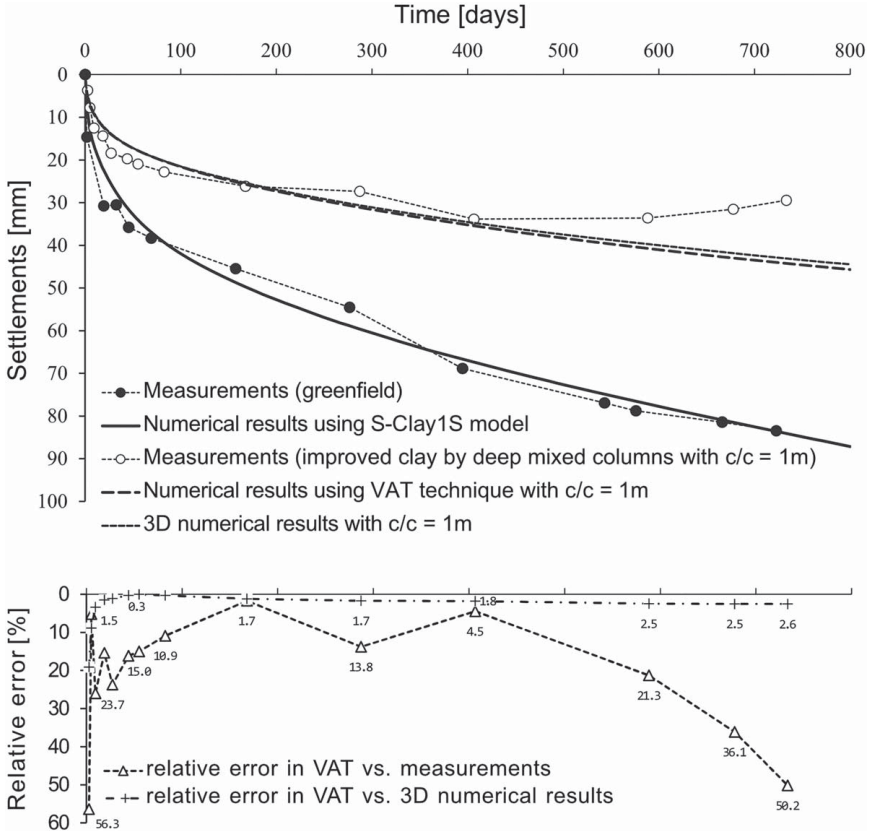

Fig. 16. VAT-predicted vertical settlement and relative error at Point A, verified against 3D calculations and validated against field measurements for a trial embankment on deep-mixed columns ($c/c = 1.0$ m).

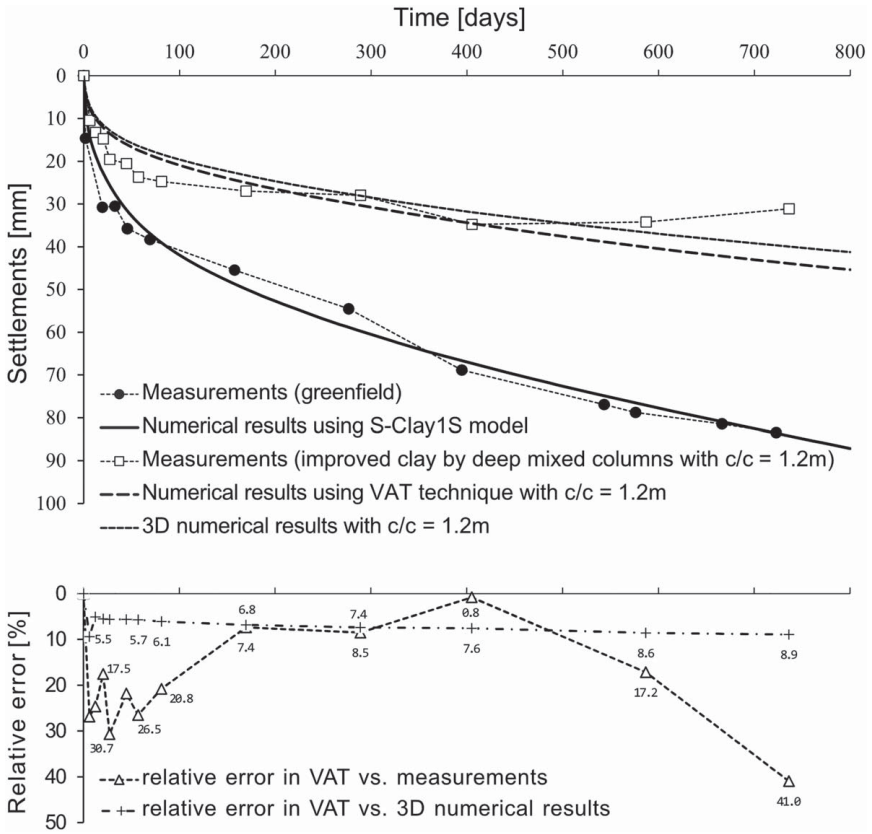

Fig. 17. VAT-predicted vertical settlement and relative error at Point A, verified against 3D calculations and validated against field measurements for a trial embankment on deep-mixed columns ($c/c = 1.2$ m).

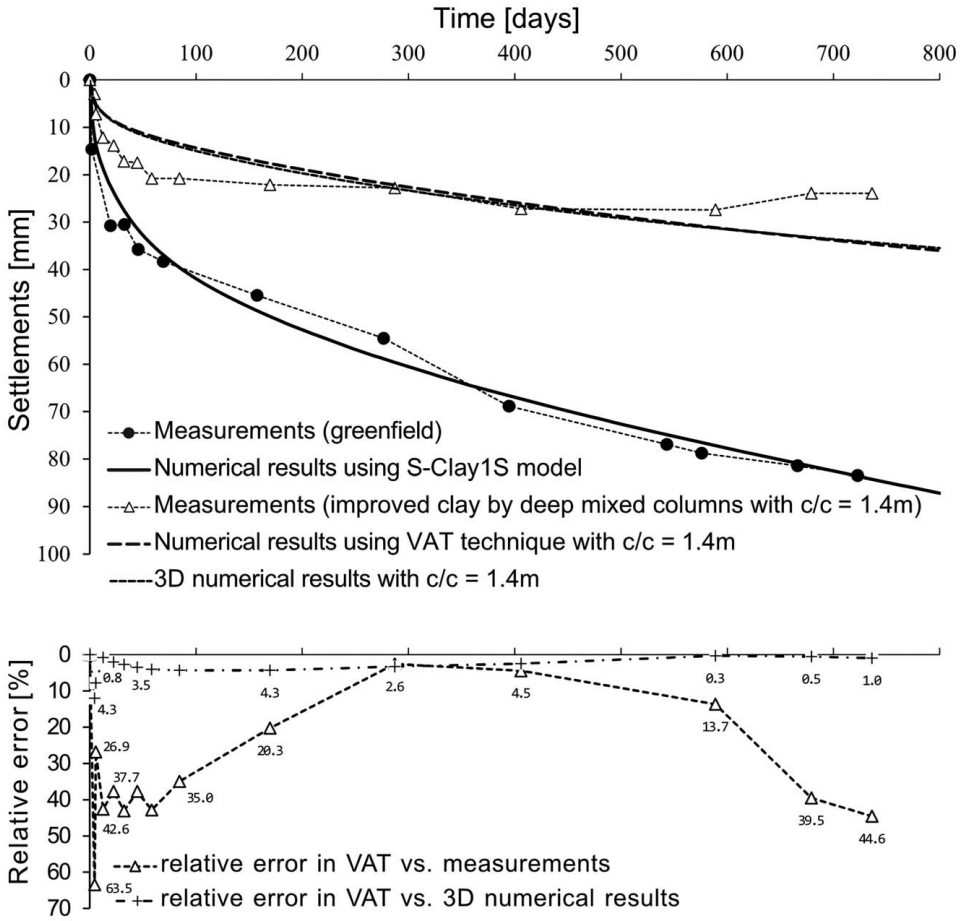

Fig. 18. VAT-predicted vertical settlement and relative error at Point A, verified against 3D calculations and validated against field measurements for a trial embankment on deep-mixed columns ($c/c = 1.4$ m).

on Fig. 2, the column volume fraction is

$$\Omega_c = \pi \frac{r_c^2}{c^2} = \pi \frac{0.3^2}{c^2}$$

which gives, for $r_c = 0.3$ m, column volume fractions of $\Omega_c = 0.283$, 0.196, and 0.144 for $c/c = 1.0$, 1.2, and 1.4 m, respectively. In fact, in the case of checking design alternatives, Ω_c will be the only changing input parameter when simulating different column diameters or spacings, reflecting one of the most powerful features of this technique. Finally, it is assumed that deep mixing cement into the natural clay will not alter the hydraulic conductivity, which is a reasonable assumption based on field observations (Bozkurt et al. 2023).

Discussion of Numerical Results

The 2D calculations with the VAT were carried out for the three different cases of column spacings, considering the geometrical differences, as listed in Table 4, among the three trial embankments (i.e., embankment width, height, and average column depth). The vertical settlements at Point A, as predicted when employing the

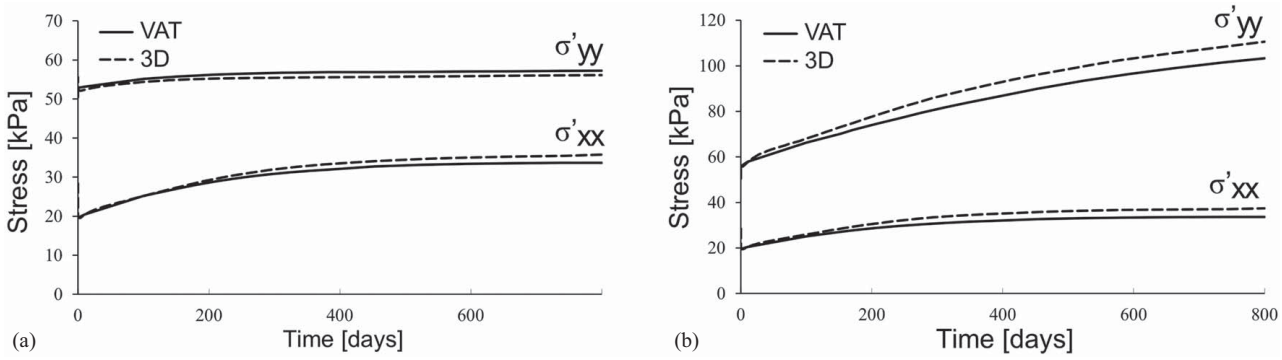

Fig. 19. VAT predictions of the vertical σ'_{yy} and horizontal σ'_{xx} effective stresses verified against the numerical results of full 3D analysis at Point B in the case of trial embankment on deep-mixed column with center-to-center spacing $c/c = 1.0$ m: (a) stresses in the natural clay; and (b) stresses in the deep-mixed column.

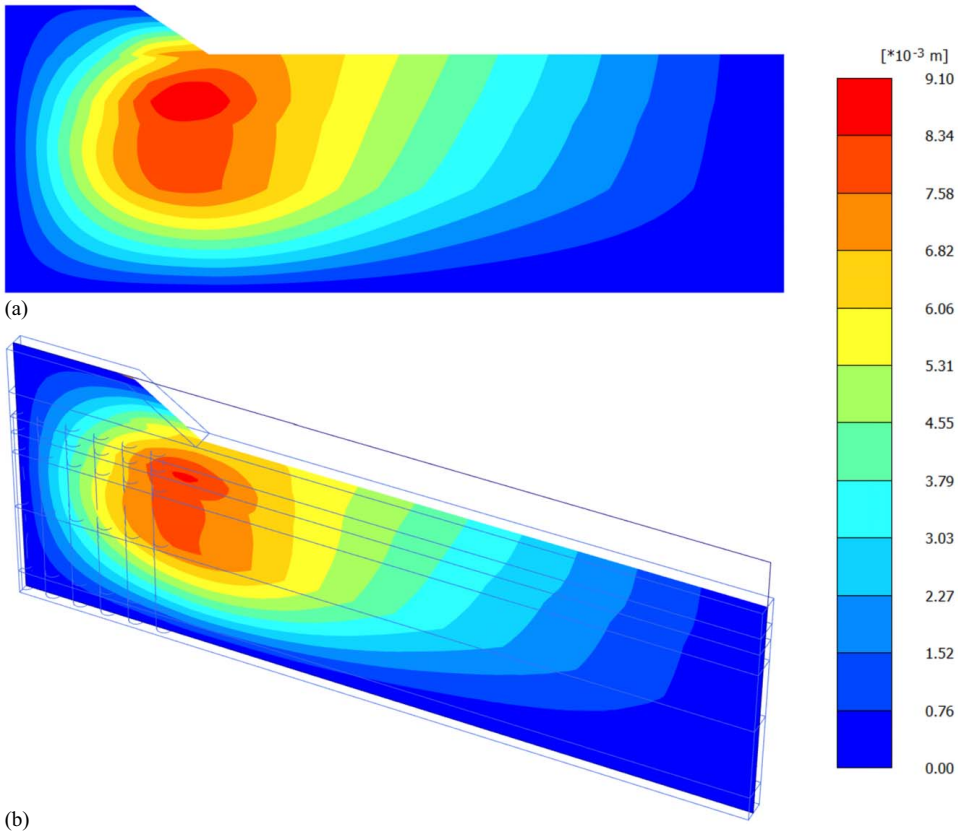

Fig. 20. Horizontal displacement map just after the construction of the embankment of mixed columns with $c/c = 1.2$ m as predicted by (a) VAT; and (b) full 3D analysis.

VAT, are compared to the measured values and the results of the full 3D calculations. Figs. 16–18 depict the results for the cases of $c/c = 1.0$, 1.2, and 1.4 m, respectively. The results of the greenfield embankment are also plotted as a reference to highlight the efficiency of the soil improvement.

For the three embankments, the VAT results accurately matched the 3D numerical results with an average relative error of about 2% for $c/c = 1$ m, 8% for $c/c = 1.2$ m, and 2% for $c/c = 1.4$ m, which verifies the method and its implementation. More importantly, the VAT was able to replicate the measured vertical settlements with sufficient accuracy for practical applications.

The deviation observed in the later stages of the experiment (i.e., after Day 600) is primarily due to the installation of embankment piles for the motorway, located about 25 m from the ramp where the test embankments are situated (Bredenberg et al. 1999). This installation affects the pore pressures in the confined aquifer, as shown in Fig. 13. The embankment in natural clay is unaffected by this (Fig. 12), unlike those on end-bearing columns (Figs.

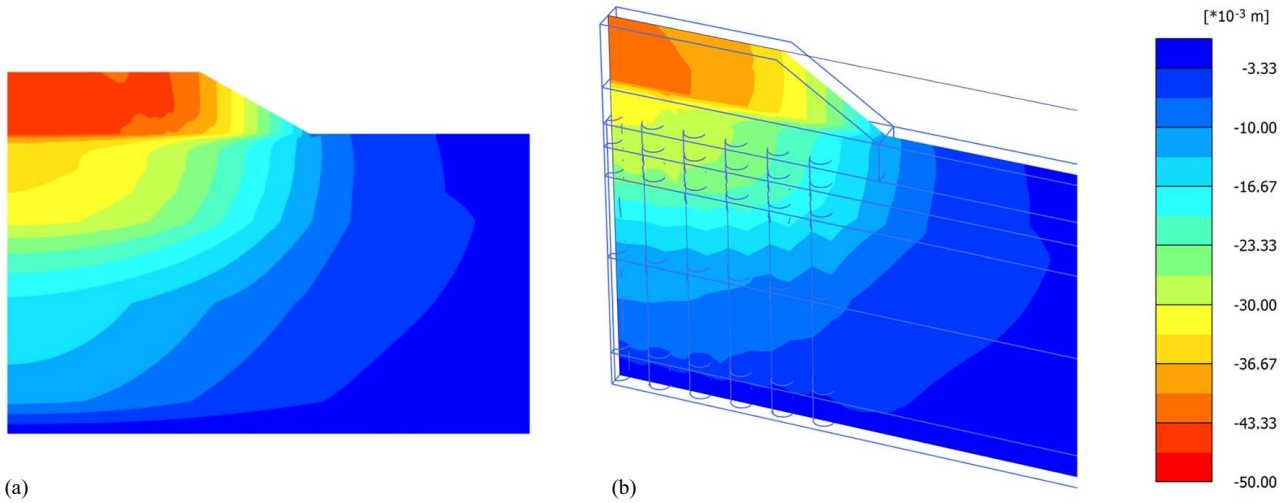

Fig. 21. Vertical displacement map after 800 days from construction of the embankment of mixed columns with $c/c = 1.2$ m as predicted by (a) VAT; and (b) full 3D analysis.

16–18), which all experience uplift. Assuming the measured settlements align with expected behavior, excluding the disturbances caused by piling activities, the average relative error across all cases would range between 5% and 8%.

Fig. 19 presents an additional verification by showing the excellent match between the evolution of effective stresses as estimated by the volume averaging technique and that calculated by the full 3D model at an arbitrary Point B (see Figs. 14 and 15 for B coordinates) in the case of $c/c = 1.0$ m.

Furthermore, Figs. 20 and 21 show the very good agreement between the settlement field (horizontal and vertical components) as predicted by the VAT and as calculated by the full 3D analysis for the case of embankment on columns with $c/c = 1.2$ m.

Conclusions

The paper introduces the volume averaging technique as a numerical tool to simplify the calculations of the complex 3D problem of embankment on deep-mixed columns. The method relies on the idea of replacing the composite system of deep-mixed columns and the surrounding natural soil by an equivalent homogenization material. Consequently, one can model a 3D problem using an equivalent 2D plane-strain model, saving a significant amount of time and effort, yet tracking the constitutive response of the constituents. The theoretical framework including the underlying assumptions of the homogenization technique was discussed, followed by the required steps for numerical implementation into a finite-element code. Finally, the trial embankments in Paimio in Finland were simulated: first as full 3D problems and then as 2D problems based on the volume averaging technique. The simulations showed that the results of the 2D analyses with the volume averaging technique perfectly match the 3D analyses, which verifies the method and the implementation. Furthermore, the volume averaging technique was able to nicely replicate the measured results of Paimio embankments, which serves as an excellent validation of the method.

It is worth noting that arching was not an issue in this study, as evidenced by the nearly perfect match between the 3D and 2D numerical calculations; however, if the investigator believes that arching may be an issue in their studied case, full 3D calculations are recommended.

For this study, the SClay1S model was used to simulate the natural clay behavior, whereas the MNHard model was used to model the behavior of the deep-mixed column. In fact, the way the method was implemented is flexible, and, in essence, it would be possible to use any constitutive model that the user finds suitable to model the column and the soil. For instance, the employed constitutive models currently do not capture the significant effect of creep, which might be tackled by using the Creep-Sclay1S model (Sivasithamparam et al. 2015; Gras et al. 2018). For columns under railway embankments, it might also be beneficial to account for the cyclic degradation of the natural soft clays, as proposed by Coelho et al. (2021). Finally, it is worth mentioning that the technique was successfully extended by Bozkurt et al. (2025) to address problems under horizontal loading, such as braced excavations stabilized with deep-mixed columns.

Data Availability Statement

Some or all data, models, or codes that support the findings of this study are available from the corresponding author upon reasonable request.

Acknowledgments

The authors would like to gratefully acknowledge Formas (Grant 2019-00456) and Swedish Transport Administration (as part of BIG, TRV 2020/46703) for funding this research. The work is done as part of the Digital Twin Cities Centre, which is supported by Sweden's Innovation Agency VINNOVA under Grant No. 2024-03904.

Notation

The following symbols are used in this paper:

A = cross-sectional area of a unit cell;
A_c = cross-sectional area of a column;
A_s = cross-sectional area of soil in a unit cell;
a = auxiliary term;
$\mathbf{B}$ = matrix of shape functions gradients;
c = center-to-center distance between deep-mixed columns;
c' = effective cohesion;
$\mathbf{D}^c$ = material stiffness matrix of the column;
$\mathbf{D}^{\text{eq}}$ = equivalent material stiffness matrix;
$\mathbf{D}^s$ = material stiffness matrix of soil;
d = variation in an internal variable;
e_o = initial void ratio;
E'_{50} = effective secant stiffness modulus;
E'_{ur} = effective unloading–reloading stiffness modulus;
E'^{ref}_{ur} = effective reference unloading–reloading stiffness modulus;
E'^{ref}_{50} = effective reference secant stiffness modulus;
err_{ij} = error per component: $i,j = 1, 2, 3$;
$\mathbf{F}$ = vector of external loading;
f = yield function;
f^s = shear yield function;
f^{MN} = Matsuoka–Nakai failure criterion;
g = plastic potential;
I_i^a = ith modified stress invariant: $i = 1, 2, 3$;
$\mathbf{K}$ = global stiffness matrix;
K_o^{OCR} = lateral earth pressure coefficient for overconsolidated state;
K_o^{NC} = lateral earth pressure coefficient for the normally consolidated state;
k = current iteration number;
k_i = hydraulic conductivity in the ith direction: $i = x, y$;
M = slope of critical state line;
m = power reflecting stiffness stress dependency;
p_{ref} = reference pressure;
p' = effective isotropic pressure;
p'_m = natural preconsolidation pressure;
p'_{mi} = intrinsic preconsolidation pressure;
q = deviatoric stress;
q_a = asymptotic deviatoric stress;
q_f = deviatoric stress at failure;
r_c = column radius;
R_f = MNHard input parameter;
$\mathbf{S}^c$ = column strain distribution matrix;
$\mathbf{S}^s$ = soil strain distribution matrix;
s_t = sensitivity;
Tol = tolerance;
$\mathbf{u}^{\text{eq}}$ = vector of equivalent displacement;
V = total volume of the unit cell; and
V_c = column volume in the unit cell.

Greek

α = inclination of the SClay1S yield surface;
α_o = initial inclination of the SClay1S yield surface;
γ = engineering shear strain;
γ_{sat} = saturated unit weight;
γ_{ij}^{c} = component ij of the engineering shear strain of the column;
γ_{ij}^{eq} = component ij of the equivalent engineering shear strain;
γ^{p} = plastic engineering shear strain;
γ_{ij}^{s} = component ij of the engineering shear strain of the soil;
γ_{50} = engineering shear strain at 50% loading till failure in the drained triaxial test;
δ = small increment;
$\boldsymbol{\varepsilon}^{c}$ = column strain vector;
ε_{ij}^{c} = component ij of the column strain;
$\boldsymbol{\varepsilon}^{\text{eq}}$ = equivalent strain vector;
$\varepsilon_{ij}^{\text{eq}}$ = component ij of the equivalent strain;
ε_{d}^{p} = plastic deviatoric strain;
ε_{v}^{p} = plastic volumetric strain;
$\boldsymbol{\varepsilon}^{s}$ = soil strain vector;
ε_{ij}^{s} = component ij of the soil strain;
ε_{50} = shear strain at 50% loading till failure in the drained triaxial test;
η = q/p' stress ratio;
$\eta_{K_o^{\text{NC}}}$ = q/p' stress ratio under K_o stress path;
κ = swelling index;
κ^{*} = modified swelling index;
λ_i = intrinsic compression index;
λ^{*} = modified compression index;
ν' = effective Poisson's ratio;
ν_c' = effective Poisson's ratio for the column material;
ξ = SClay1S parameter;
ξ_d = SClay1S parameter;
σ_i^{a} = modified principal stress;
$\boldsymbol{\sigma}^{c'}$ = column effective stress vector;
$\sigma_{ij}^{c'}$ = component ij of the column effective stress;
$\boldsymbol{\sigma}^{\text{eq}'}$ = equivalent effective stress;
$\sigma_{ij}^{\text{eq}'}$ = component ij of the equivalent effective stress;
$\sigma_{ij}^{\text{out}'}$ = component ij of the out-of-balance effective stress;
$\boldsymbol{\sigma}^{s'}$ = soil effective stress vector;
$\sigma_{ij}^{s'}$ = component ij of the soil effective stress;
φ' = effective internal friction angle;
φ_{cv}' = internal friction angle at the critical state;
φ_m = mobilized friction angle;
χ = bonding parameter;
χ_o = initial bonding parameter;
ψ' = dilatancy angle;
ψ_m' = mobilized dilatancy angle;
ω = SClay1S parameter;
ω_d = SClay1S parameter;
Δ = increment;
Ω_c = column volume fraction;
Ω_s = soil volume fraction;
$\langle\rangle$ = Macaulay brackets;
$\|$ = absolute value; and
$(\cdot)$ = time derivative.

References

Aalto, A. 2003. "Full scale tests in the field using dry mixing method." In *Proc., Int. Workshop on Geotechnics of Soft Soils—Theory and Practice*, 505–510. Essen, Germany: European Research Training Network SCMEP, Verlag Glückauf Essen, Yrittäjäruuvi Oy.

Abed, A. 2008. *Numerical modeling of expansive soil behavior*. Stuttgart, Germany: Instituts für Geotechnik (IGS).

Abed, A., L. Korkiala-Tanttu, J. Forsman, and K. Koivisto. 2021. "3D simulations of deep mixed columns under road embankment." *Raken. Mek.* 54: 1–20.

Balaam, N. P., and J. R. Booker. 1981. "Analysis of rigid rafts supported by granular piles." *Int. J. Numer. Anal. Methods Geomech.* 5 (4): 379–403. https://doi.org/10.1002/nag.1610050405.

Becker, P., and M. Karstunen. 2013. *Volume averaging technique in numerical modelling of floating deep mixed columns in soft soils*. Boca Raton, FL: CRC Press.

Becker, P., and M. Karstunen. 2014. "Volume averaging technique for modelling deformations in soft soil improved with deep mixed columns." In *Proc., Int. Conf. on Piling and Deep Foundations*. Sweden: European Federation of Foundation Contractors (EFFC).

Benz, T. 2007. "Small-strain stiffness of soils and its numerical consequences." Ph.D. thesis, Institut für Geotechnik, Univ. of Stuttgart.

Borja, R. I., and S. R. Lee. 1990. "Cam-clay plasticity, part 1: Implicit integration of elasto-plastic constitutive relations." *Comput. Appl. Mech. Eng.* 78 (2): 49–72. https://doi.org/10.1016/0045-7825(90)90152-C.

Bozkurt, S., A. Abed, and M. Karstunen. 2023. "Finite element analysis for a deep excavation in soft clay supported by lime-cement columns." *Comput. Geotech.* 162: 105687. https://doi.org/10.1016/j.compgeo.2023.105687.

Bozkurt, S., A. Abed, and M. Karstunen. 2025. "Homogenisation method for braced excavations stabilised with deep-mixed columns." *Comput. Geotech.* 181: 107095. https://doi.org/10.1016/j.compgeo.2025.107095.

Bredenberg, H., B. B. Broms, and G. Holm. 1999. *Dry mix methods for deep soil stabilization*. Boca Raton, FL: CRC Press.

Broms, B. B., and P. Boman. 1979. "Lime columns—A new foundation method." *J. Geotech. Eng. Div.* 105 (4): 539–556. https://doi.org/10.1061/AJGEB6.0000788.

Canetta, G., and R. Nova. 1989. "A numerical method for the analysis of ground improved by columnar inclusions." *Comput. Geotech.* 7 (1–2): 99–114. https://doi.org/10.1016/0266-352X(89)90009-8.

Coelho, B. Z., J. Dijkstra, and M. Karstunen. 2021. "Viscoplastic cyclic degradation model for soft natural soils." *Comput. Geotech.* 135: 104176. https://doi.org/10.1016/j.compgeo.2021.104176.

De Borst, R., and O. M. Heeres. 2002. "A unified approach to the implicit integration of standard, non-standard and viscous plasticity models." *Int. J. Numer. Anal. Methods Geomech.* 26: 1059–1070. https://doi.org/10.1002/nag.234.

Drucker, D. C., and W. Prager. 1952. "Soil mechanics and plastic analysis or limit design." *Q. Appl. Math.* 10 (2): 157–165. https://doi.org/10.1090/qam/48291.

Duncan, J. M., and C.-Y. Chang. 1970. "Nonlinear analysis of stress and strain in soils." *J. Soil Mech. Found. Div.* 96 (5): 1629–1653. https://doi.org/10.1061/JSFEAQ.0001458.

EuroSoilStab. 2002. *Development of design and construction methods to stabilise soft organic soils: design guide soft soil stabilisation*. CT97-0351. Project No. BE 96-3177. Watford, UK: Industrial & Materials Technologies Programme (Brite- EuRam III), European Commission.

Gens, A., and Nova, A. 1993. "Conceptual bases for a constitutive model for bonded soils and weak rocks." In *Proc., Int. Symp. on Geotechnical Engineering of Hard Soils-Soft Rocks*. Rotterdam, The Netherlands: A.A. Balkema.

Gras, J.-P., N. Sivasithamparam, M. Karstunen, and J. Dijkstra. 2018. "Permissible range of model parameters for natural fine-grained materials." *Acta Geotech.* 13: 387–398.

Karstunen, M., H. Krenn, S. J. Wheeler, M. Koskinen, and R. Zentar. 2005. "Effect of anisotropy and destructuration on the behavior of Murro test embankment." *Int. J. Geomech.* 5 (2): 87–97. https://doi.org/10.1061/(ASCE)1532-3641(2005)5:2(87).

Karstunen, M., C. Wiltafsky, H. Krenn, F. Scharinger, and H. F. Schweiger. 2006. "Modelling the behaviour of an embankment on soft clay with different constitutive models." *Int. J. Numer. Anal. Methods Geomech.* 30 (10): 953–982. https://doi.org/10.1002/nag.507.

Kondner, R. L., and J. S. A. Zelasko. 1963. "Hyperbolic stress–strain formulation for sands." In *Proc., 2nd Pan American on Soil Mechanics*

and Foundation Engineering, 289–324. São Paulo, Brazil: Associação Brasileira de Mecânica dos Solos.

Koskinen, M., M. Karstunen, and S. J. Wheeler. 2002. "Modelling destructuration and anisotropy of a natural soft clay." In *Proc., 5th European Conf. on Numerical Methods in Geotechnical Engineering*, 11–19. Paris, France: Presses de l'ENPC/LCPC.

Lee, J.-S. 1993. *Finite element analysis of structured media*. Swansea, UK: Univ. College of Swansea.

Lee, J. S., and G. N. Pande. 1998. "Analysis of stone-column reinforced foundations." *Int. J. Numer. Anal. Methods Geomech.* 22 (12): 1001–1020. https://doi.org/10.1002/(SICI)1096-9853(199812)22:12<1001::AID-NAG955>3.0.CO;2-I.

Matsuoka, H., and T. Nakai. 1982. "A new failure criterion for soils in three dimensional stresses." In *Proc., IUTAM Conf. on Deformation and Failure of Granular Materials*, 253–263. Rotterdam, The Netherlands: A.A. Balkema.

Rowe, P. W. 1962. "The stress-dilatancy relation for static equilibrium of an assembly of particles in contact." *Proc. R. Soc. Lond. Ser. Math. Phys. Sci.* 269: 500–527.

Savila, I.-M. E., L. K. Korkiala-Tanttu, J. A. Forsman, and M. S. Löfman. 2025. "Mechanical properties of stabilized soil: Study on recovered field samples from deep stabiliz*ation sites." Transp. Geotech.* 51: 101540. https://doi.org/10.1016/j.trgeo.2025.101540.

Schofield, A., and P. Wroth. 1968. *Critical state soil mechanics*. New York: McGraw-Hill.

Schweiger, H. F. 1989. "Finite element analysis of stone column reinforced foundations." Ph.D. thesis, Univ. of Wales, Swansea, Wales.

Schweiger, H. F., and G. N. Pande. 1986. "Numerical analysis of stone column supported foundations." *Comput. Geotech.* 2 (6): 347–372. https://doi.org/10.1016/0266-352X(86)90030-3.

Schweiger, H. F., and G. N. Pande. 1989. "Modelling stone column reinforced soil—A modified Voigt approach." In *Proc., 3rd Int. Symp. on Numerical Models in Geomechanics. NUMOG III*, *Niagara Falls, Canada*. New York: Elsevier Applied Science.

Sivasithamparam, N., M. Karstunen, and P. Bonnier. 2015. "Modelling creep behaviour of anisotropic soft soils." *Comput. Geotech.* 69: 46–57. https://doi.org/10.1016/j.compgeo.2015.04.015.

Sloan, S. W., A. J. Abbo, and D. Sheng. 2001. "Refined explicit integration of elastoplastic models with automatic error control." *Eng. Comput.* 18 (1–2): 121–194. https://doi.org/10.1108/02644400110365842.

Vepsäläinen, P., and O. Arkima. 1992. *The arching of road embankments. Final report*. Research Rep. No. 4/1992. Helsinki, Finland: Finnish National Road Administration.

Vepsäläinen, P., O. Arkima, M. Lojander, and A. Näätänen. 1991. "The trial embankments in Vaasa and Paimio, Finland." In *Proc., Xth European Conf. on Soil Mechanics and Foundation Engineering*, 633–640. Rotterdam, The Netherlands: A.A. Balkema.

Vogler, U. 2008. *Numerical modelling of deep mixing with volume averaging technique*. London: Univ. Strathclyde.

Vogler, U., and M. Karstunen. 2008. "Application of volume averaging technique in numerical modelling of deep mixing." In *Geotechnics of soft soils: Focus on ground improvement*, edited by K. Minna and L. Martino, 201–208. Boca Raton, FL: CRC Press.

Vogler, U., and M. Karstunen. 2007. "Numerical modelling of deep mixed columns with volume averaging technique." In *Proc., 10th Int. Symp. on Numerical Models in Geomechanics (NUMOG X)*, 495–502. Oxford, UK: Taylor & Francis Ltd.

Wheeler, S. J., M. Karstunen, and A. Näätänen. 1999. "Anisotropic hardening model for normally consolidated soft clays." In *Proc. NUMOG VII*, 33–40. Oxford, UK: Taylor & Francis Ltd.

Wheeler, S. J., A. Näätänen, M. Karstunen, and M. Lojander. 2003. "An anisotropic elastoplastic model for soft clays." *Can. Geotech. J.* 40 (2): 403–418. https://doi.org/10.1139/t02-119.

Wood, D. M. 1990. *Soil behaviour and critical state soil mechanics*. Chicago: Cambridge University Press.